A Robust Analytical Sensitivity Analysis for Coupled Aero-Structural Systems

Koorosh Gobal*, Ramana V. Grandhi†

Wright State University, Dayton, Ohio 45324

Christopher M. Koehler‡

U.S. Air Force Research Laboratory, Wright-Patterson Air Force Base, Ohio 45433

In this research, a continuum sensitivity formulation for the shape sensitivity analysis of a coupled fluid-structure system is derived. The flow field is modeled using Navier-Stokes equations and the solid domain is represented as a linear elastic model. The conventional approach to this problem is based on a body-conformal grid to represent the solid boundaries. However, these methods fail for complex shapes and/or large deformations of the solid region. This issue can be addressed by using the immersed boundary method, where additional force terms are added to the governing equations to represent the solid boundaries. Using this approach, significant computational saving is achieved by two means: 1) Highly efficient solvers can be utilized on Cartesian grids, and 2) Mesh deformation is not necessary. The sensitivity analysis consists of differentiating the continuum form of the governing equations. In this approach the sensitivity and governing equations use the same differential operators. Therefore same solver is utilized for both systems of equations. Proposed methodology is used to solve a 2D flow over a cylinder and a simplified aeroelastic wing model. The sensitivity of flow field around and on the cylinder, airfoil lift, and wing structural responses are calculated with respect to shape parameters. High-fidelity computational fluid dynamics (CFD) is used to solve the flow problem and wing structure is represented with a linear finite element model. The sensitivity results are verified using the complex step method where a good agreement is realized.

I. Introduction

Fluid-structure interaction (FSI) play prominent roles in many scientific and engineering fields, yet a comprehensive study of such problems remains a challenge due to their strong coupling, nonlinearity and complexity in simulation of high-fidelity physics. For most FSI problems, analytical solutions are impossible to obtain, whereas physical experiments are limited in scope. Thus, to investigate the fundamental physics involved in the complex interaction between fluids and solids, numerical simulations are employed. These techniques are based on coupled computational fluid dynamics (CFD) approaches for solving the flow problem and finite element analysis (FEA) for calculating the structural responses. Nevertheless, lack of computational resources and lengthy simulation times have been the major issues in the coupled FSI analysis. This makes the use of finite difference sensitivities for the development and design optimization of large scale aerospace vehicles. Furthermore, the inaccuracy of finite differencing could result in convergence difficulties and inaccurate optimum results.

Formulation of the analytical sensitivity methods requires derivation of analytic sensitivity equations. These equations are obtained by differentiating the governing equations with respect to design variables such as shape of the boundaries. Among various available methods, the discrete analytic sensitivity is a popular approach. This method is based on differentiating the discretized system of governing equations [1]. In order to differentiate the discretized system of equations, it is necessary to modify the source-code of the black-box CFD/FEA solvers [2]. This might not be possible due to lack of availability and the complexity of modifying source codes. Moreover, the discrete model has high costs, especially in terms of operation costs and memory requirements [3].

The Continuum sensitivity analysis (CSA), involves solving a set of partial differential equations named the continuum sensitivity equations (CSEs) to get the analytical sensitivities. CSA has several computational efficiencies that other sensitivity formulations lack. Aurora and Haug [4], followed by Dems and Mroz [5], were among the first to introduce CSA for structural prob-

*Graduate Research Assistant, Department of Mechanical and Materials Engineering, AIAA Student Member; gobal.2@wright.edu.

†Distinguished Research Professor, AIAA Fellow.

‡Research Engineer, Multidisciplinary Science and Technology Center.

lems. Stanley and Stewart [6] applied CSA in a fluid mechanics discipline with a goal for aerodynamic design. Pelletier and Etienne have applied CSA to numerous fluid-structure interaction (FSI) problems [7] focused mainly on sensitivities of fluid flow parameters near the structure. Liu and Canfield have employed CSA for shape optimization of nonlinear structures subject to an aeroelastic gust response [8]. They used the finite element method to solve the potential flow around an airfoil and applied CSA to find the airfoil pressure coefficient sensitivity with respect to the maximum camber. In these works, body conforming grids were used to model the flow around the solid bodies. The conforming mesh methods consider the interface conditions as physical boundary conditions, which treat the interface location as part of the solution and requires meshes that conform to the interface. Owing to the movement and/or deformation of the solid structure, re-meshing (or mesh-updating) is needed as the solid boundaries move. Although conforming mesh methods have been widely used in many FSI problems, they are cumbersome, if not impossible, to apply to problems with large deformations [9]. Moreover, when performing sensitivity analysis on a deforming mesh, it is required to calculate the mesh sensitivities as well [10]. This adds to the computational cost of calculating sensitivities. The shortcoming of a robust grid generation and the additional cost of calculating mesh sensitivities motivated an important research effort to develop a method that does not require fluid domain mesh modification for the optimization iterations.

The non-conforming mesh methods treat the boundary location as constraints imposed on governing equations. As a result, the fluid and solid equations can be conveniently solved independently from each other on their respective grids and re-meshing is not necessary. The distinction between these two types of meshes can be observed in Figure 1, where a solid body (a sphere) is moving in a fluid domain.

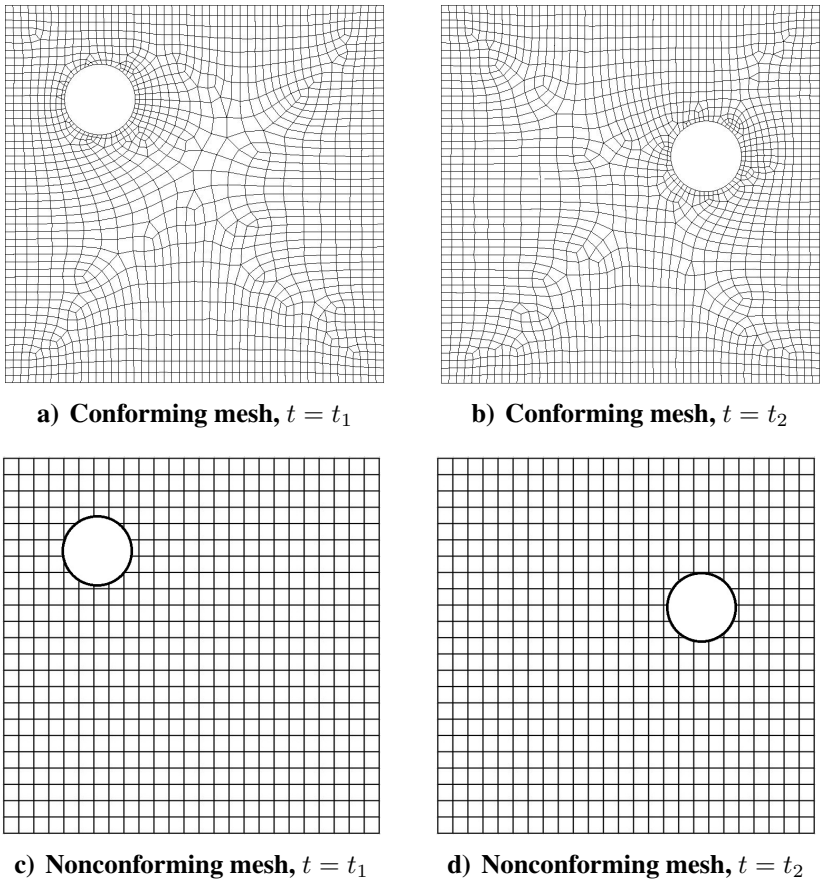

a) Conforming mesh, $t = t_1$ **b) Conforming mesh,** $t = t_2$

c) Nonconforming mesh, $t = t_1$ **d) Nonconforming mesh,** $t = t_2$

Figure 1. Example of conforming and nonconforming mesh.

Most non-conforming mesh techniques are based upon the framework of the immersed boundary methods. The basic idea here is to employ a numerically efficient Cartesian grid for the discretization of the fluid domain and to represent the immersed fluid-solid interface by modifying the governing equations. This can be formulated as additional source terms in the momentum equation and can be performed in the continuous domain, i.e. before discretization, or by altering the linear system resulting from discretization in time and space, which is termed discrete forcing [11]. The immersed boundary method is very appealing, since it relieves the user from the task of grid generation that can be extremely difficult and tedious for complex configurations. In the immersed boundary method, the boundary of an immersed solid is tracked by Lagrangian markers that are convected by a fluid. Numerically, the communication between the solid and the fluid is obtained by spreading singular forces from the Lagrangian markers to nearby Cartesian grid nodes and interpolating the velocity from nearby Cartesian grid nodes to the Lagrangian markers with

the use of discrete Dirac δ functions.

In recent years, the immersed boundary method has been applied to multiple FSI problems. Choi et al. calculated the surface pressure coefficients for high Reynolds number flow around an NACA0012 airfoil [12]. Fadlun et al. investigated the capability of this method to simulate high-Reynolds number turbulent flows in complex geometries. They chose an axisymmetric piston-cylinder assembly with a fixed central valve for this purpose [13]. Mittal et al. developed a sharp interface immersed boundary method for simulating incompressible viscous flow over three-dimensional immersed bodies. They applied it to a highly complex three-dimensional moving body of bluegill sunfish [14]. Their method was based on a discrete-forcing scheme that allows for a sharp representation of the immersed boundary. Vanella et al. tested the accuracy of immersed boundary method for the case of two falling plates. Most research that has been done on the immersed boundary focused on the analysis aspects of the method and the sensitivity analysis has not been extensively studied. There has been limited research on the application of immersed boundary method for optimization of the internal flows where the penalization technique was used to optimize the shape of the channels for fluid flow [15, 16]; however, the developed methodology is only applicable to low Reynolds number flows and does not provide good accuracies near the solid boundaries.

In this research, we use the continuum sensitivity analysis to calculate the sensitivity of coupled FSI problems to shape parameters, where the flow is modeled using steady, laminar, incompressible Navier-Stokes equations. We used high fidelity CFD simulation to solve the flow equations and linear FEA model for the structure. The fluid-solid interaction is modeled using the continuum immersed boundary method which is capable of sharp representation of the solid boundaries. The traditional immersed boundary method uses a discrete Dirac function for transferring data between domains. This is not applicable when using continuum sensitivity analysis since the governing equations need to be continuously differentiable. Therefore, a continuous regularized delta function is developed to satisfy this need. The methodology is applied to flow over a cylinder and a wing model for a coupled aero-structure representation. The analytical sensitivities of flow and structural response are calculated with respect to shape parameters with CSA and verified using

the complex step method.

II. Numerical Approach

A. Immersed Boundary Formulation

Viscous and incompressible flow in a Cartesian square domain Ω containing an immersed boundary, as shown in Figure (2), is modelled by the Navier-Stokes equations:

$$\rho\left[\frac{\partial\vec{V}}{\partial t}+\vec{\nabla}\cdot\left(\vec{V}\otimes\vec{V}\right)\right]=-\vec{\nabla}P+\mu\nabla^2\vec{V}+\vec{F} \tag{1a}$$

$$\vec{\nabla}\cdot\vec{V}=0 \tag{1b}$$

where ρ is density; μ is dynamic viscosity; $\vec{V}$ is fluid's velocity; and P is the fluid pressure. The forcing function, $\vec{F}$ is given by

$$\vec{F}(\vec{x},t)=\int_{\Omega}\vec{f}(\vec{x}_k,t)\delta(\vec{x}-\vec{x}_k)d\vec{x}_k \tag{2}$$

where $\delta(\vec{x}-\vec{x}_k)$ is a Dirac delta function; $\vec{x}_k$ are the locations of Lagrangian points placed over the immersed boundary; $\vec{f}(\vec{x}_k)$ is the Lagrangian force density; and $\vec{F}(\vec{x})$ is the Eulerian force that has non-zero values only over the immersed boundary. The Lagrangian force terms are calculated using virtual boundary formulation that is proposed by Goldstein [17], to simulate turbulent flow over a riblet-covered surface and to address other similar problems. The main idea of this method is to treat the embedded boundary by adding a force field to the fluid, in such away that the fluid takes the same velocity as the solid surface. Since the force field is not known a priori, it must be calculated in a feedback way as shown in Equation (3). This model involves two imposed constants, α and β, which are chosen to be both negative and large enough in magnitude to bring the fluid velocity close to the interface velocity. The feedback forcing function $\vec{f}(\vec{x}_k,t)$ is given as

$$\vec{f}\left(\vec{x}_k,t\right)=\alpha\int_0^t\left[\vec{u}\left(\vec{x}_k,t\right)-\vec{U}\left(\vec{x}_k,t\right)\right]dt+\beta\left[\vec{u}\left(\vec{x}_k,t\right)-\vec{U}\left(\vec{x}_k,t\right)\right] \tag{3}$$

where $\vec{u}\left(\vec{x}_k,t\right)$ is the response variable value from the Eulerian analysis calculated at the La-

grangian nodes. $\vec{U}(\vec{x}_k, t)$ is the desired value of $\vec{u}(\vec{x}_k, t)$ as the corresponding Lagrangian nodes, $\vec{x}_k$. For the case of a no-slip boundary condition ($\vec{U}(\vec{x}_k, t) = 0$) the forcing function in Equation (3) tries to bring the velocity to zero on the boundary. $\vec{u}(\vec{x}_k, t)$ is calculated from its neighbouring Eulerian nodes by using the same delta function used in Equation (2).

$$\vec{u}(\vec{x}_k, t) = \int_\Omega \vec{u}(\vec{x}, t)\delta(\vec{x} - \vec{x}_k)d\vec{x} \tag{4}$$

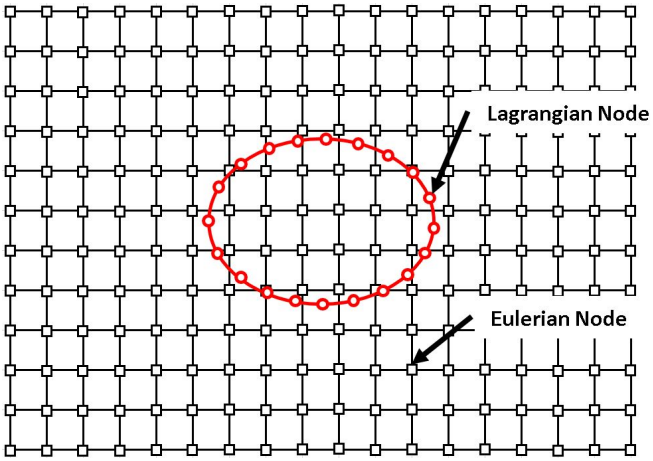

Figure 2. Immersed boundary illustration

Shin et al. investigated the stability of virtual boundary formulation for various types of regularized delta functions [18]. These functions have have different bandwidth which corresponds to the number of Eulerian points where the effect of forcing function is distributed as shown in Figure 3. The higher bandwidth for the delta function results in smearing effect near the boundaries. In continuum sensitivity analysis approach, the governing equations are differentiated to get the sensitivity equations. Therefore, it is required for the delta functions to have continuous derivative. This is not true for the 2, 3, and 4 point delta functions shown in Figure 3 as they have piecewise continuous derivatives. This results in stability issues for the solution of sensitivity equations. We propose the following regularized delta function formulation that satisfies this need.

$$\delta_h(\vec{x}) = \frac{1}{h^3}\phi\left(\frac{x - x_k}{h}\right)\phi\left(\frac{y - y_k}{h}\right)\phi\left(\frac{z - z_k}{h}\right) \tag{5}$$

where h is the distance between the Eulerian nodes. ϕ is defined as:

$$\phi(r) = \frac{e^{-r}}{(1+e^{-r})^2} \quad , \quad r = \frac{x - x_k}{h} \tag{6}$$

As shown here, the proposed function in Equation (5) is $\mathcal{C}^1$ continuous and it has lower bandwith to ensure the accuracy of the results near the boundary.

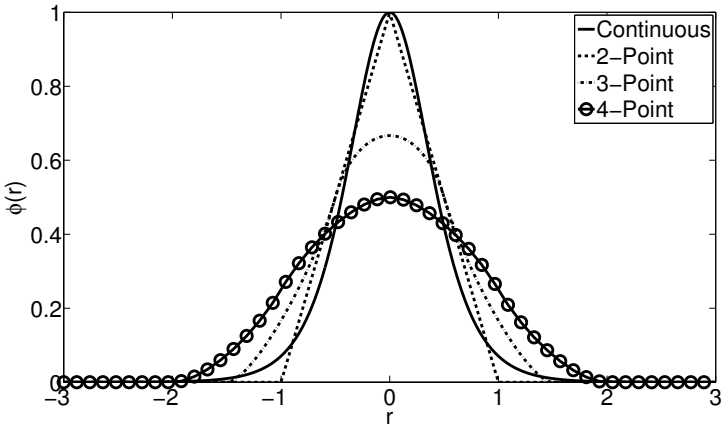

Figure 3. Comparison between the different delta function formulation.

Finally, the forcing function, $\vec{F}(\vec{x})$, can be written by combining equations (2), (3), and (4).

$$\begin{aligned}\vec{F}(\vec{x},t) = \int_\Omega \Bigg\{ \alpha \int_0^t \left[\int_\Omega \vec{u}(\vec{x},t)\delta(\vec{x}-\vec{x}_k)d\vec{x} - \vec{U}\left(\vec{x}_k,t\right) \right] dt + \\ \beta \left[\int_\Omega \vec{u}(\vec{x},t)\delta(\vec{x}-\vec{x}_k)d\vec{x} - \vec{U}\left(\vec{x}_k,t\right) \right] \Bigg\} \delta(\vec{x}-\vec{x}_k)d\vec{x}_k\end{aligned} \tag{7}$$

In Equation (7), the integrals on the domain, Ω, transfer the data between the Lagrangian and Eulerian domains. The inner integrals, map the velocities from Eulerian to Lagrangian nodes to calculate the force at Lagrangian node, $\vec{f}\,(\vec{x},t)$. The outer integral maps the forcing function from the Lagrangian to Eulerian nodes where the governing equations are solved (Figure 4).

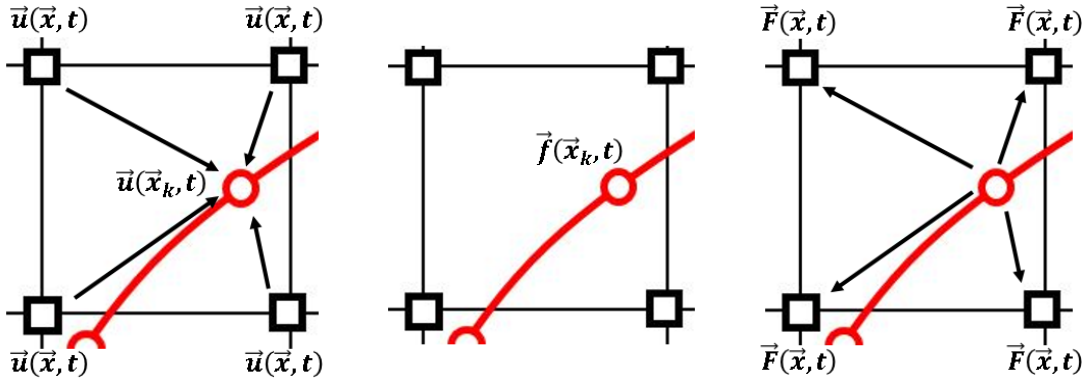

a) Velocity calculation at the Lagrangian node. **b) Forcing function evaluation.** **c) Forcing function transfer to the Eulerian nodes.**

Figure 4. Data transfer between Eulerian and Lagrangian nodes.

B. Analytic Sensitivity Formulation

Figure 5 represents the domain, Ω, in the Cartesian space. This domain is the union of the solid, Ω_s, and fluid, Ω_f, domains where the Navier-Stokes equations are solved. The boundary conditions which are defined on the sides of this domain, Γ, are not affected by the design variables. By using this approach, the boundaries of the solid domain are added to the fluid's governing equations as mentioned in the previous section.

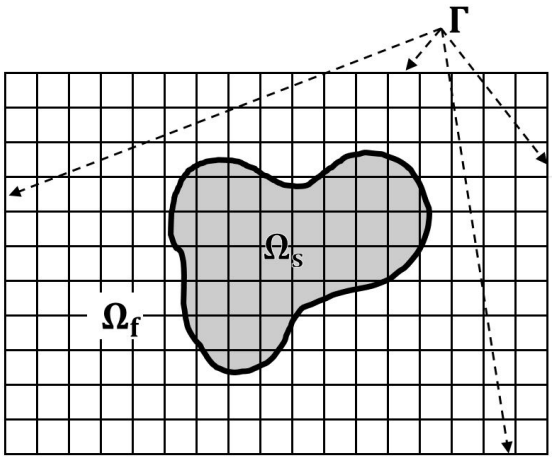

Figure 5. Computational domain, $\Omega = \Omega_f \cup \Omega_s$, with boundary of Γ

The governing equation and boundary conditions are written in the general form as

$$A(\vec{u},\vec{b}) = f(\vec{x},t;\vec{b}) \quad \text{on} \quad \Omega \tag{8a}$$

$$B(\vec{u}, \vec{b}) = g(\vec{x}, t; \vec{b}) \quad \text{on} \quad \Gamma \tag{8b}$$

where A and B are the differential operators for the governing equations and the boundary conditions respectively, and $\vec{u}$ is the vector of response variables. These can be displacements in structural mechanics or velocities and pressures in fluid dynamics. $\vec{x}$ and $\vec{b}$ are vectors of spatial coordinates and design variables, respectively. The total sensitivity of response variable $\vec{u}$ to the i-th design variable b_i is calculated as

$$\frac{D\vec{u}}{Db_i} = \frac{\partial \vec{u}}{\partial b_i} + \frac{\partial \vec{u}}{\partial \vec{x}} \cdot \frac{\partial \vec{x}}{\partial b_i} \tag{9}$$

This material derivative consists of the local design derivative, $\frac{\partial \vec{u}}{\partial b_i}$, plus a convective term, $\frac{\partial \vec{u}}{\partial \vec{x}} \cdot \frac{\partial \vec{x}}{\partial b_i}$. The local design derivative is a measure of how much the response at a point changes due to change in the design parameter. The convective term tracks the movement of the material point when the spatial coordinates will change with the design variable. The geometric domain is a function of design variable in the case of conformal meshes as shown in Figure 1. However, for the case of non-body conformal meshes, the spatial coordinates will not change as the design parameter varies. Therefore, the convective term is equal to zero [19]; this means that the local and total forms of the sensitivities are equal.

The local sensitivity equations are derived by partial differentiation of Equation (1) along with its boundary conditions. The differentiation to i-th design variable, b_i, yields the following equation for the sensitivity analysis:

$$\rho \left[\frac{\partial \vec{V'}}{\partial t} + \vec{\nabla} \cdot \left(\vec{V'} \otimes \vec{V} + \vec{V} \otimes \vec{V'} \right) \right] = -\vec{\nabla} P' + \mu \nabla^2 \vec{V'} + \vec{F'} \tag{10a}$$

$$\vec{\nabla} \cdot \vec{V'} = 0 \tag{10b}$$

In the above equation, $\vec{V'}$ and P' are the local sensitivities of the velocity and pressure to i-th design variable, b_i, respectively. $\vec{V}$ is calculated from the solution of the governing equation (1). Comparing equations (1) and (10), we can see that the form of the governing and sensitivity equations are the same. Therefore, we can use the same solver for solving both of these equations.

This is not possible when using the discrete formulation for the sensitivity analysis.

The effect of boundary movement is introduced in Equation (10) through $\vec{F'}$, more specifically throughout the derivative of the regularized delta function to design variable, b_i. The derivative of the forcing function is derived as

$$\begin{aligned}\vec{F'}(\vec{x},t) = \int_\Omega \Bigg\{ \alpha \int_0^t \left[\int_\Omega \vec{u'}(\vec{x},t)\delta(\vec{x}-\vec{x}_k)d\vec{x} - \int_\Omega \vec{u}(\vec{x},t)\frac{\partial\delta(\vec{x}-\vec{x}_k)}{\partial\vec{x}_k}\frac{\partial\vec{x}_k}{\partial b_i}d\vec{x}\right] dt + \\ \beta\left[\int_\Omega \vec{u'}(\vec{x},t)\delta(\vec{x}-\vec{x}_k)d\vec{x} - \int_\Omega \vec{u}(\vec{x},t)\frac{\partial\delta(\vec{x}-\vec{x}_k)}{\partial\vec{x}_k}\frac{\partial\vec{x}_k}{\partial b_i}d\vec{x}\right]\Bigg\}\delta(\vec{x}-\vec{x}_k)d\vec{x}_k + \\ \int_\Omega \Bigg\{ \alpha \int_0^t \left[\int_\Omega \vec{u}(\vec{x},t)\delta(\vec{x}-\vec{x}_k)d\vec{x} - \vec{U}\left(\vec{x}_k,t\right)\right] dt + \\ \beta\left[\int_\Omega \vec{u}(\vec{x},t)\delta(\vec{x}-\vec{x}_k)d\vec{x} - \vec{U}\left(\vec{x}_k,t\right)\right]\Bigg\}\frac{\partial\delta(\vec{x}-\vec{x}_k)}{\partial\vec{x}_k}\frac{\partial\vec{x}_k}{\partial b_i}d\vec{x}_k\end{aligned} \tag{11}$$

where $\vec{u'}\left(\vec{x},t\right)$ is the sensitivity of velocity to design parameter, b_i. As shown in the above equation, we used the chain rule to differentiate the regularized delta function with the design variable, b_i. The shape of the design variable only affects the location of the Lagrangian points. The derivative of the Lagrangian nodes, $\vec{x}_k$, to b_i can be easily calculated by the problem definition since the dependency of the shape of the domain (Lagrangian nodes) and design variables are known. The derivative of the regularized delta function to the Lagrangian node, x_k, is calculated analytically by differentiating Equation (6). This results in a system of differential equations for the sensitivity response of the system. This method has a significant advantage to the conventional approaches, since there is no need to calculate the sensitivity of the boundary condition or computational mesh to the design variable. In the next section, we apply this methodology to two different problems.

III. Demonstration Results

In this section, we will show applications of the continuum sensitivity analysis of flow response to shape design variables. In these problems, the immersed solid boundaries are modelled using the immersed boundary approach as discussed in the previous section. We consider two demonstration problems: 1) flow over a cylinder 2) one-way fluid-structure coupling of flow over an airfoil. The

flow is modelled as an incompressible, viscous, and laminar flow. The governing equations are discretized as shown in Equation (12).

$$\frac{\vec{V}^{n+1}-\vec{V}^{n}}{\Delta t}+\left(\frac{3}{2}N\vec{V}^{n}-\frac{1}{2}N\vec{V}^{n-1}\right)=-Gp^{n+1/2}+\frac{1}{2Re}\left(L\vec{V}^{n+1}+L\vec{V}^{n}\right)+\vec{F}^{n} \tag{12a}$$

$$D\vec{V}^{n+1}=0 \tag{12b}$$

In this equation, $\vec{V}$ is the velocity vector; p is the pressure; Re is the Reynolds number; $\vec{F}$ is the momentum forcing applied to enforce the no-slip boundary condition along the immersed boundary; N is the discrete convective operator; G is the discrete gradient operator; L is the discrete Laplacian operator; and D is the discrete divergence operator. Here, n denotes the nth time step and Δt denotes the time increment. The discrete spatial operators N, G, L, and D are evaluated using the second-order central finite-difference scheme. The numerical method is based on the Navier-Stokes solver, adopting the fractional-step method and a staggered Cartesian grid system. As shown above, the force terms are treated explicitly. We use the projection approach to solve this coupled system of equations [20].

In the following demonstration problems, we used the complex step method to verify the sensitivity results [21]. Complex step differentiation is a technique that employs complex arithmetic to obtain the numerical value of the first derivative of a real valued analytic function of a real variable, avoiding the loss of precision inherent in traditional finite differences. The complex step derivative is calculated as follows:

$$\mathcal{F}'\left(u;b\right)=\frac{\mathrm{Im}\left[\mathcal{F}\left(u;b+ih\right)\right]}{h} \tag{13}$$

This means that we perturb the design variable by an imaginary value of ih and then look at the imaginary portion of the resulting response divided by h. Using the complex step method, we can choose a small step size for h without loosing accuracy. Sensitivity of an analytical function in the form $F(x)=\dfrac{e^{x}}{\cos^{3}x+\sin^{3}x}$ at $x=\pi/4$ for complex step and finite difference methods are shown in Figure 6. As shown here, the nomalized error in the finite difference calculation increases

as the step size becomes smaller.

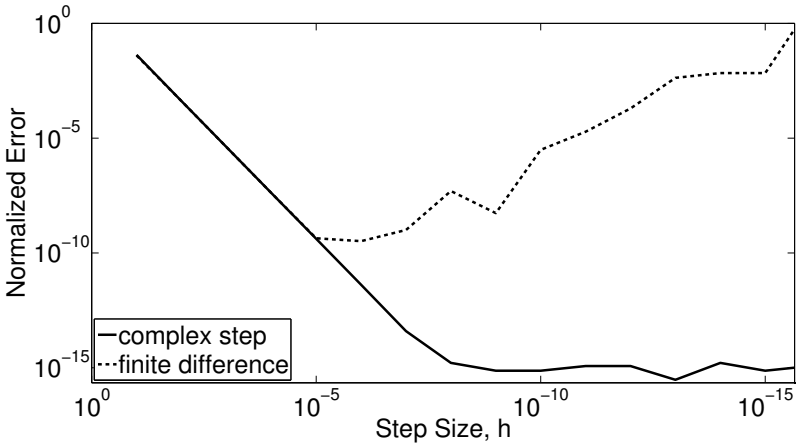

Figure 6. Relative error in the sensitivity estimates of the finite-difference and the complex-step methods using the analytic result as the reference. Normalized error = $\left|F' - F'_{ref}\right| / F'_{ref}$

A. Flow Over a Cylinder

We modelled the flow around a cylinder and calculated the sensitivity of the flow to the cylinder radius. The domain is defined as a rectangle with length and height of 2 meters and 1 meter respectively, as shown in Figure 7. The cylinder radius is selected as 0.1 meter and located 1 meter from the inlet. The inlet boundary condition is defined as constant velocity and the outlet is modelled as an outflow boundary condition. This means that the gradient of u and v velocities are zero at the outlet. The top and bottom walls are modelled as free-slip boundary conditions. The flow is modelled by choosing the Reynolds number as 100 and 1000. The boundary of the cylinder is modelled using 100 Lagrangian nodes. The flow results and mesh convergence study for different Reynolds numbers are shown in Figure 8. For this analysis, the α and β parameter of Equation (3) are selected as -10^4 and -50 respectively. As shown in Figure 8, the forcing function satisfied the zero velocity condition on the surface of the cylinder.

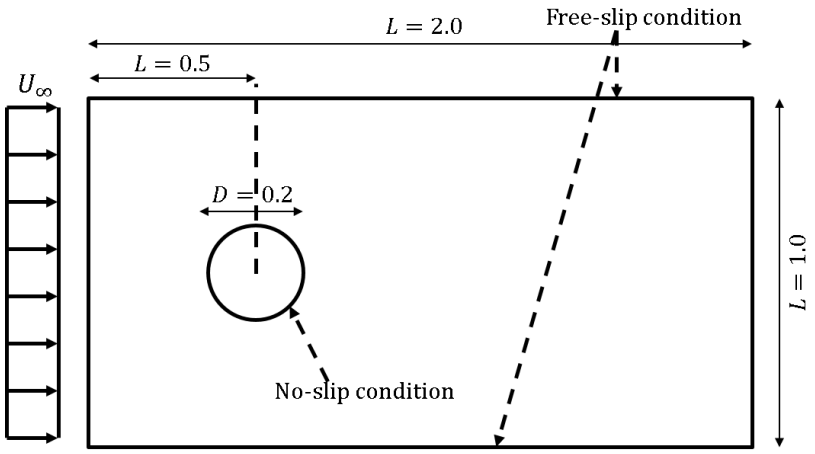

Figure 7. Physical domain for flow over circular cylinder.

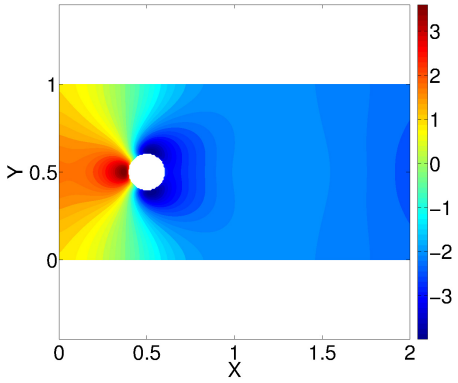

a) Pressure contour for $Re = 100$

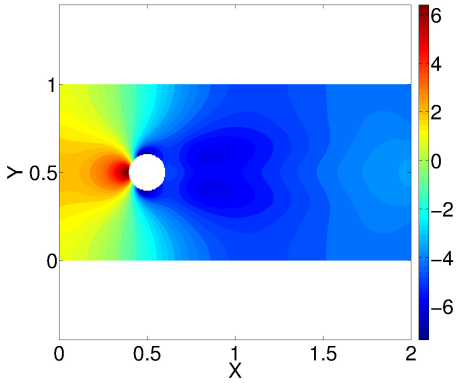

b) Pressure contour for $Re = 1000$

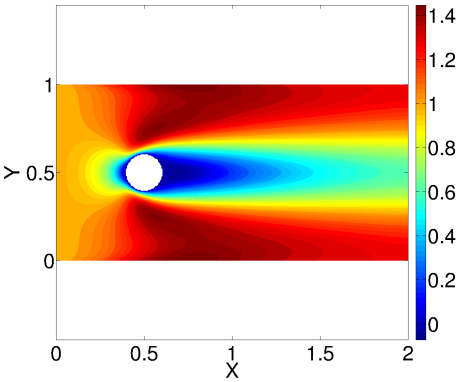

c) Velocity contour for $Re = 100$

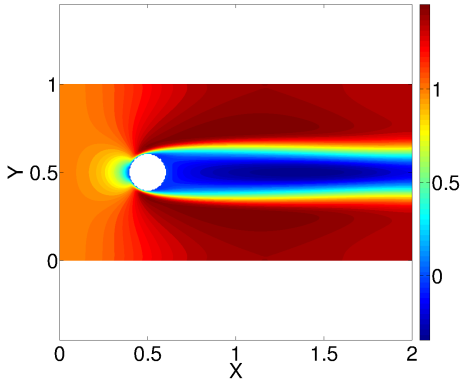

d) Velocity contour for $Re = 1000$

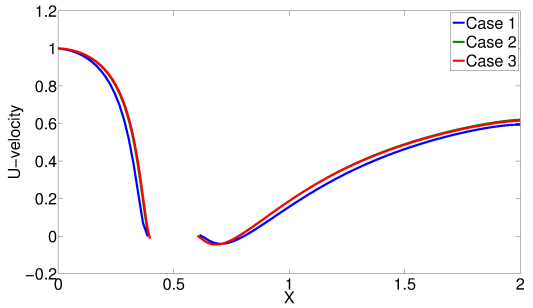

e) U-velocity on $y = 0.5$ **for different number of mesh nodes for** $Re = 100$**.**

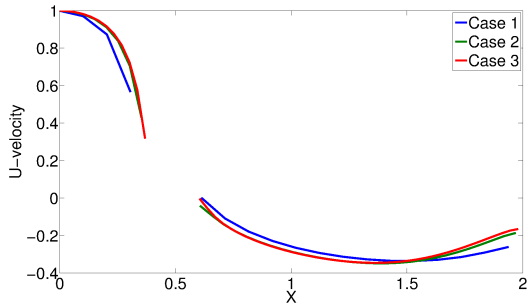

f) U-velocity on $y = 0.5$ **for different number of mesh nodes for** $Re = 1000$

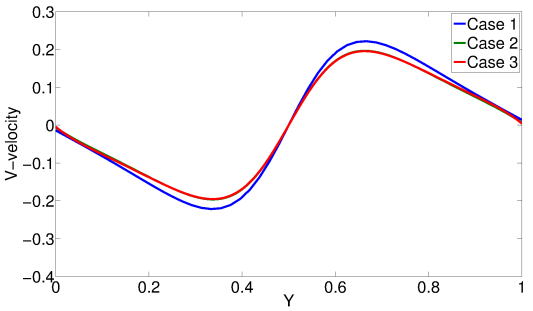

g) V-velocity on $x = 0.25$ **for different number of mesh nodes for** $Re = 100$

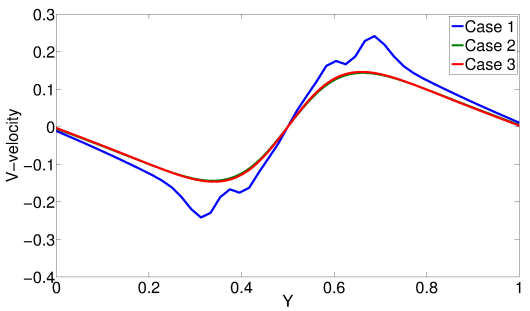

h) V-velocity on $x = 0.25$ **for different number of mesh nodes for** $Re = 1000$

Figure 8. Results of convergence study for flow over cylinder. Case 1, case 2, and case 3 are domains with 100×50**,** 200×100**,** 300×150 **nodes.**

The time history of force terms on the surface of the cylinder are shown in Figure 9. We choose five probe locations on the surface to track the force values. It should be noted that these are the force terms added to the Navier-Stokes equations to represent the boundary, not the forces acting on the surface of the cylinder due to hydrodynamic pressure. As shown in Figure 9, the values of the forcing function starts oscillating at the beginning and reaches a steady-state value. This indicates that we reached a steady-state solution.

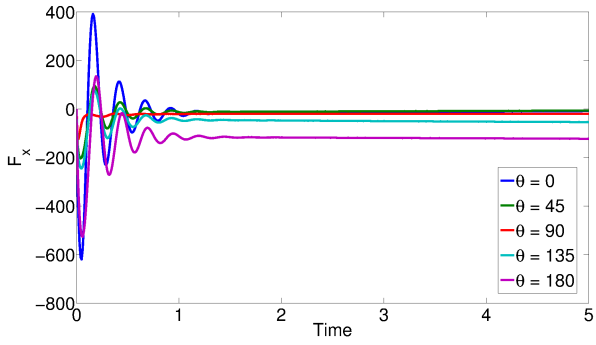

a) Forcing term in x direction.

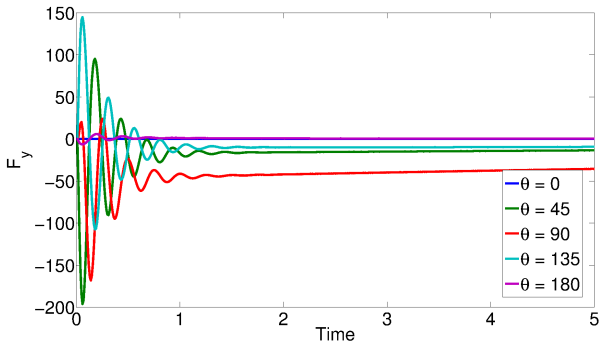

b) Forcing term in y direction.

Figure 9. Forcing terms on the surface of the cylinder. $\theta = 0$ is on the front and $\theta = 180$ is on the back of the cylinder for Re = 100.

The sensitivity contour plots for the pressure and velocity for different values of Reynolds numbers are shown in Figures 10 and 11. As shown here, the contour plots for the continuum sensitivity analysis and complex step results agree well with each other.

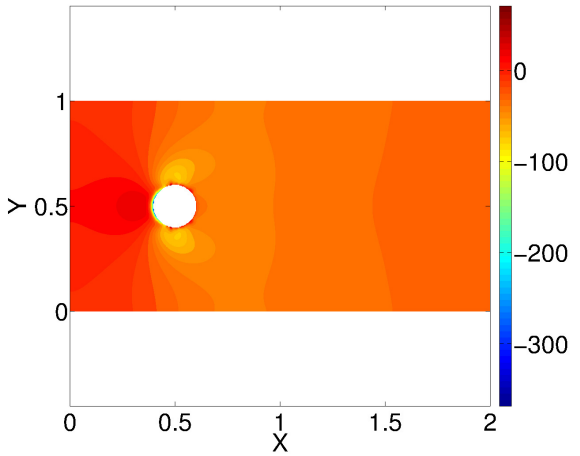

a) Continuum sensitivity result for pressure sensitivity

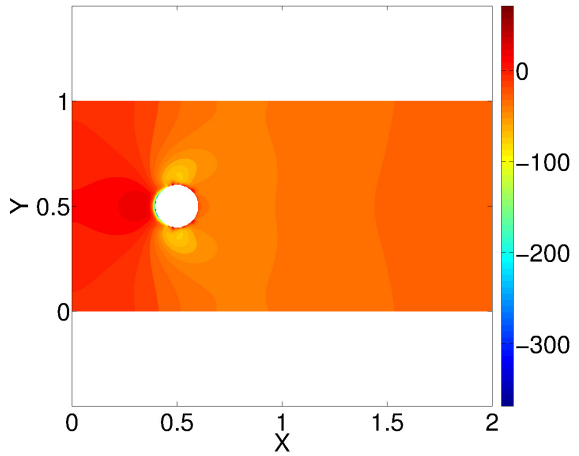

b) Complex step result for pressure sensitivity

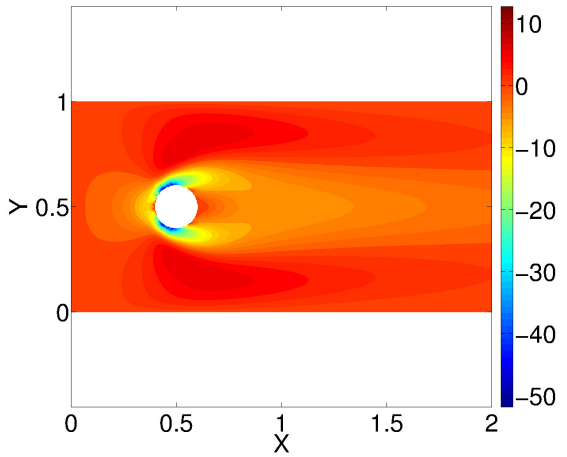

c) Continuum sensitivity result for u-velocity sensitivity

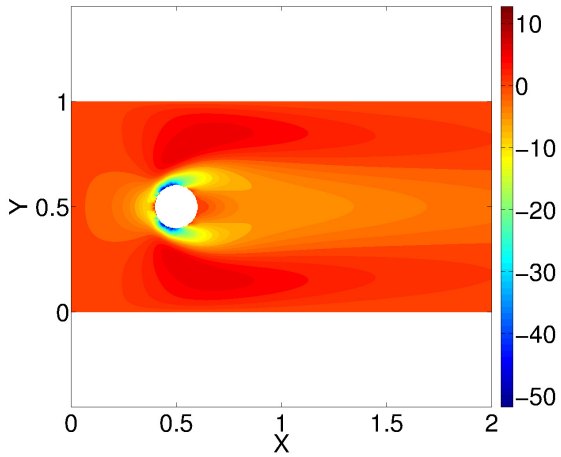

d) Complex step result for u-velocity sensitivity

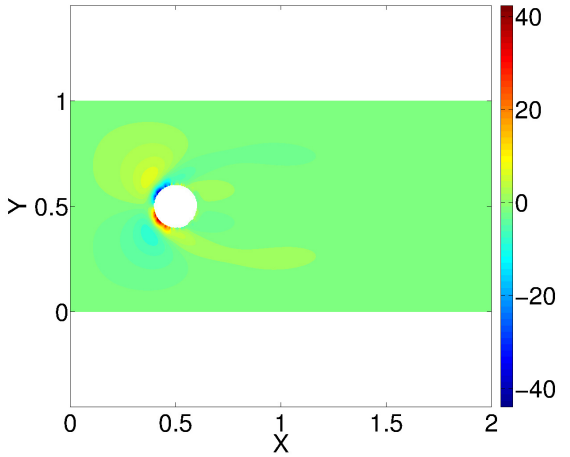

e) Continuum sensitivity result for v-velocity sensitivity

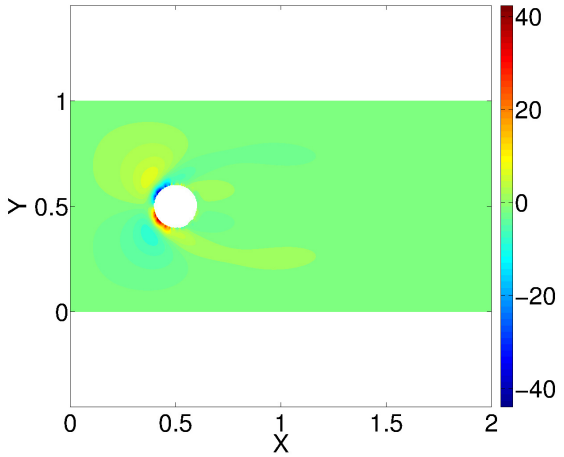

f) Complex step result for v-velocity sensitivity

Figure 10. Comparison of sensitivity contours for flow over cylinder, $Re = 100$.

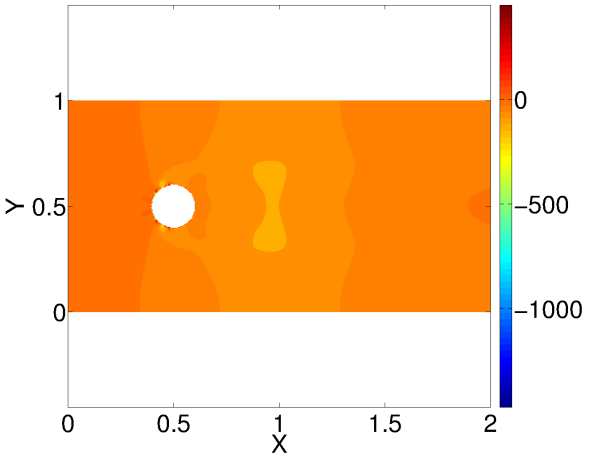

a) Continuum sensitivity result for pressure sensitivity

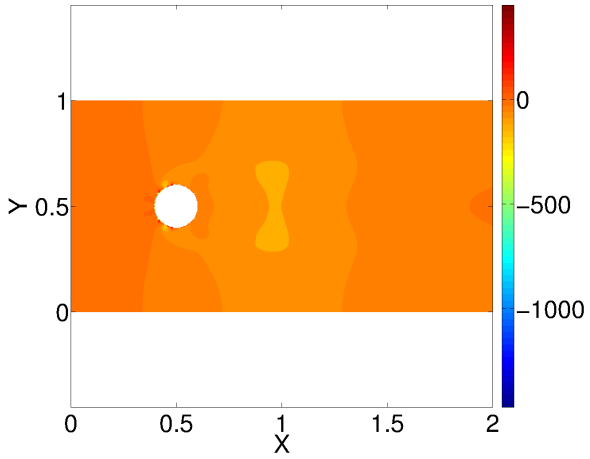

b) Complex step result for pressure sensitivity

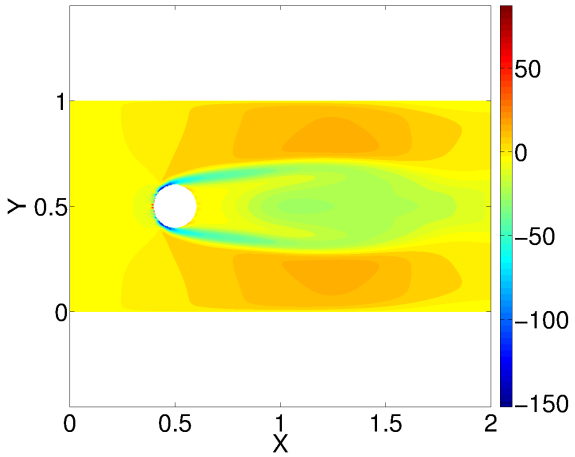

c) Continuum sensitivity result for u-velocity sensitivity

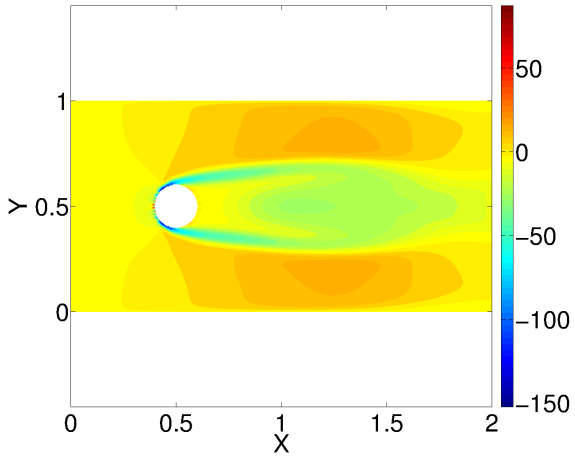

d) Complex step result for u-velocity sensitivity

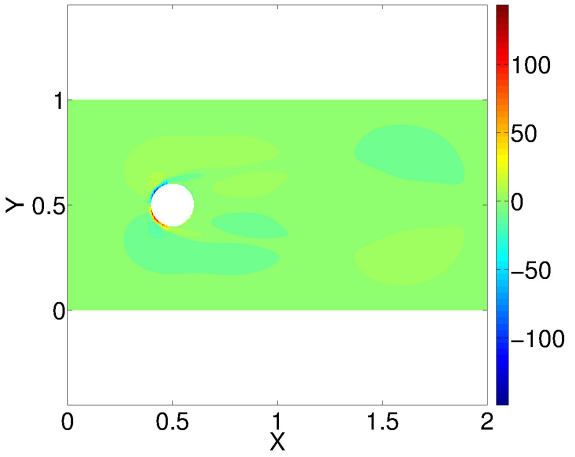

e) Continuum sensitivity result for v-velocity sensitivity

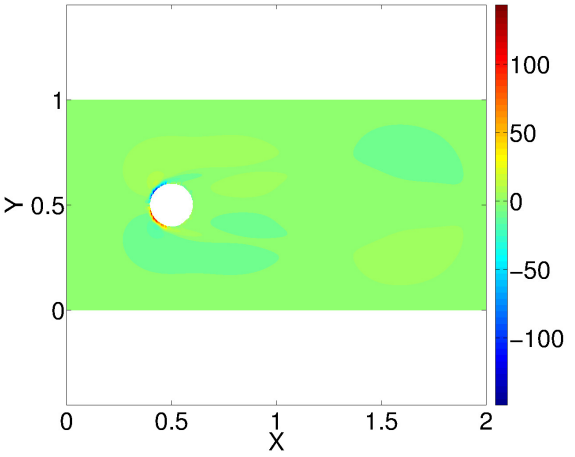

f) Complex step result for v-velocity sensitivity

Figure 11. Comparison of sensitivity contours for flow over cylinder, $Re = 1000$.

For a better comparison between the sensitivity results of continuum sensitivity analysis and complex step methods, we looked at different locations in the computational domain. These locations are indicated in Figure 12.

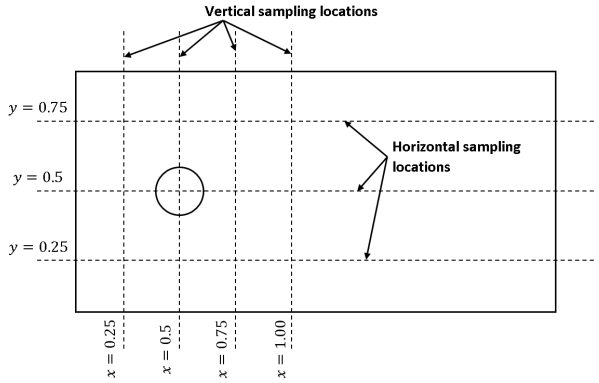

Figure 12. Sampling locations for the sensitivities

We compared the sensitivity of u-velocity and pressure on sample locations for different values of Reynolds numbers. As shown in Figures 13 and 14, the continuum sensitivity and complex step results agree well with each other.

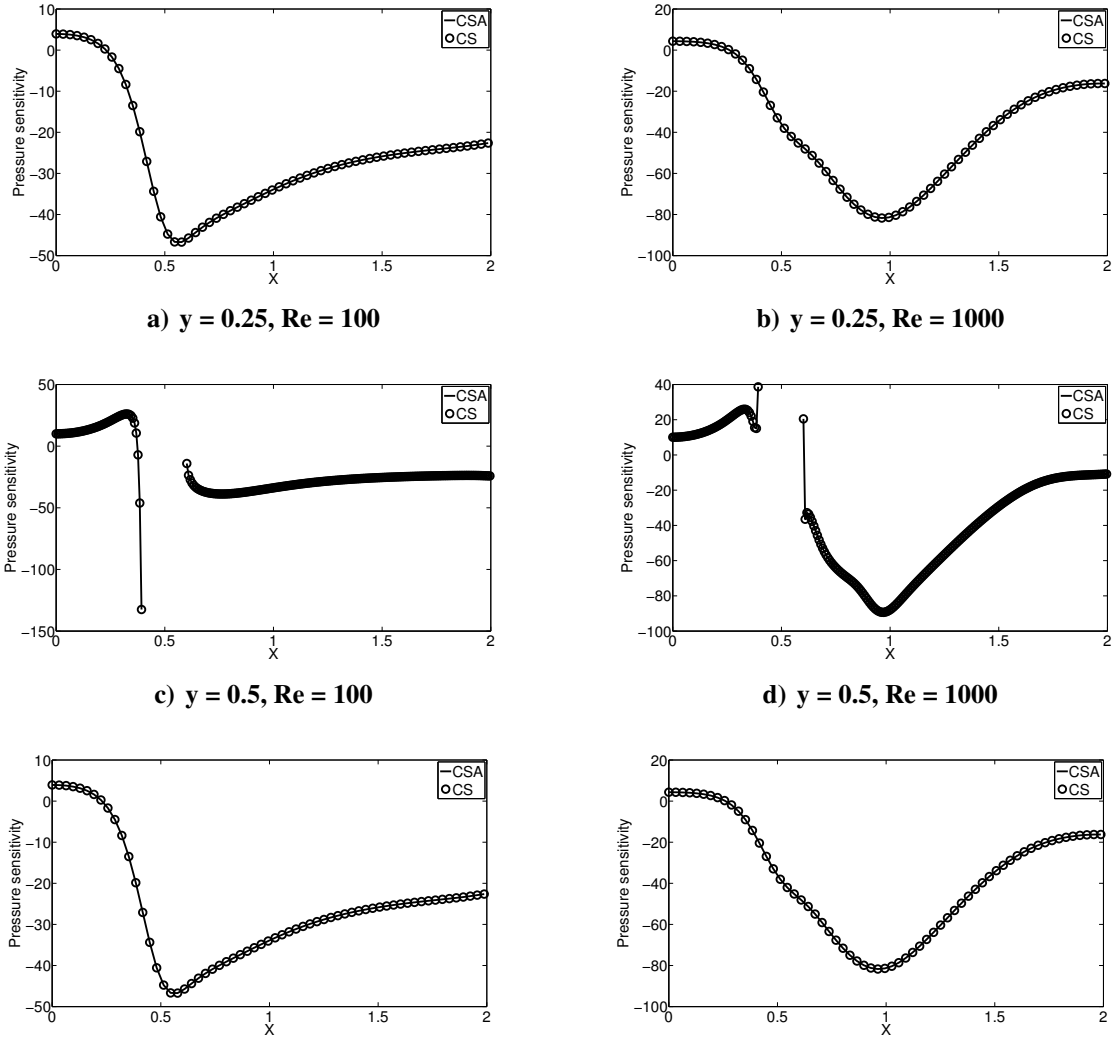

a) y = 0.25, Re = 100

b) y = 0.25, Re = 1000

c) y = 0.5, Re = 100

d) y = 0.5, Re = 1000

e) y = 0.75, Re = 100

f) y = 0.75, Re = 1000

Figure 13. Pressure sensitivity to cylinder radius for different Reynolds numbers on horizontal sampling line.

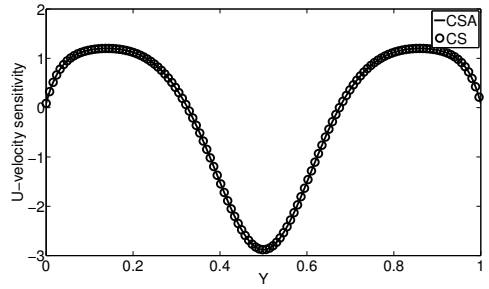

a) x = 0.25, Re = 100

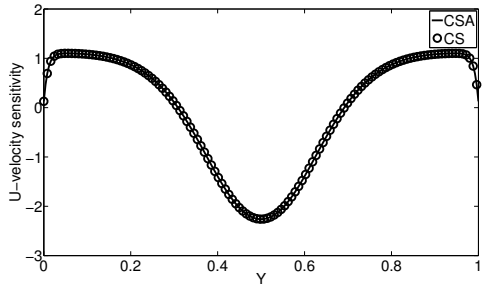

b) x = 0.25, Re = 1000

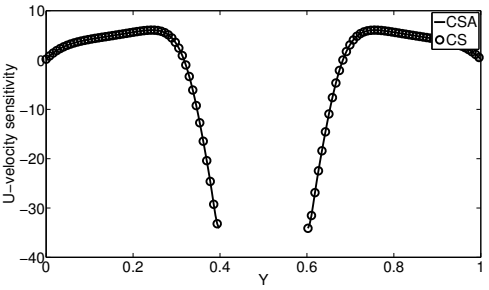

c) x = 0.5, Re = 100

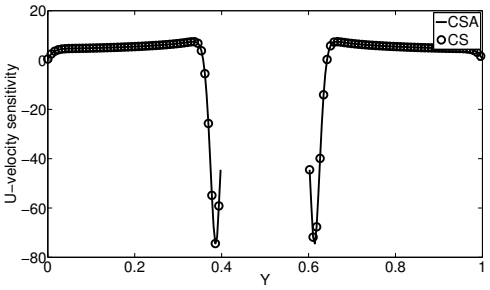

d) x = 0.5, Re = 1000

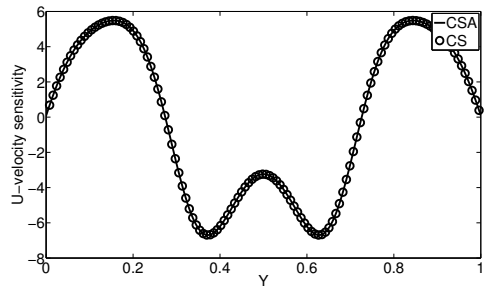

e) x = 0.75, Re = 100

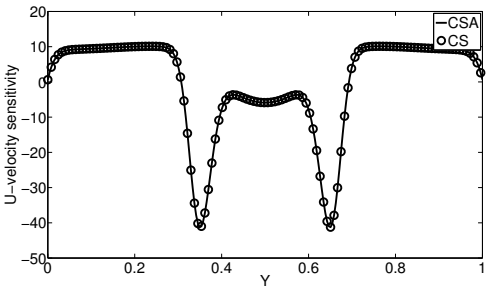

f) x = 0.75, Re = 1000

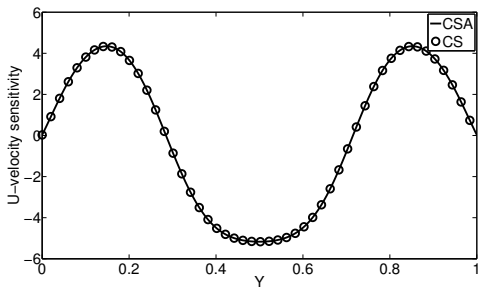

g) x = 1.00, Re = 100

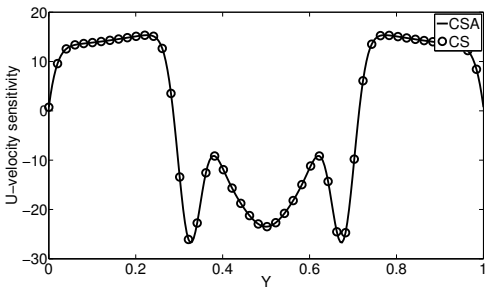

h) x = 1.00, Re = 1000

Figure 14. U-velocity sensitivity to cylinder radius for different Reynolds numbers on vertical sampling line.

B. Linear Beam with an Airfoil

Laminar flow over a simplified wing is selected as the second demonstration problem. The physical model for this problem is shown in Figure 15. The one-way fluid-solid interaction is defined by mounting the airfoil on an elastic beam where the flow is caluclated using a CFD simulation. The load and moment from the aerodynamic analysis are transferred to the structure through the mounting point. The beam is $4\ m$ in length, with a cross-sectional area of $0.002\ m^2$, and modulus of elasticity of 200 GPa. The initial angle of attack is selected at 2 degrees. The fluid is modeled as laminar and incompressible flow using Navier-Stokes equations. The Reynolds number for the flow is selected as 100 for this problem. The boundary conditions are defined as the inflow velocity and zero gradient of velocity at the outlet. The top and bottom walls are modelled as free-slip boundary conditions. The structure is modelled as a linear Euler-Bernoulli beam. We are interested in calculating the sensitivity of the tip displacement of the structure to the shape of the airfoil.

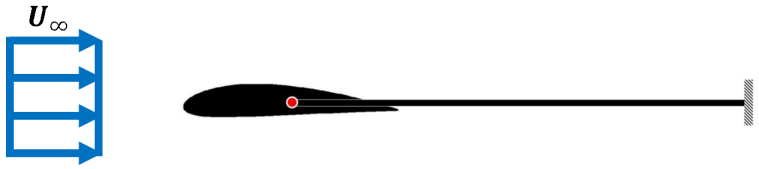

a) Physical domain

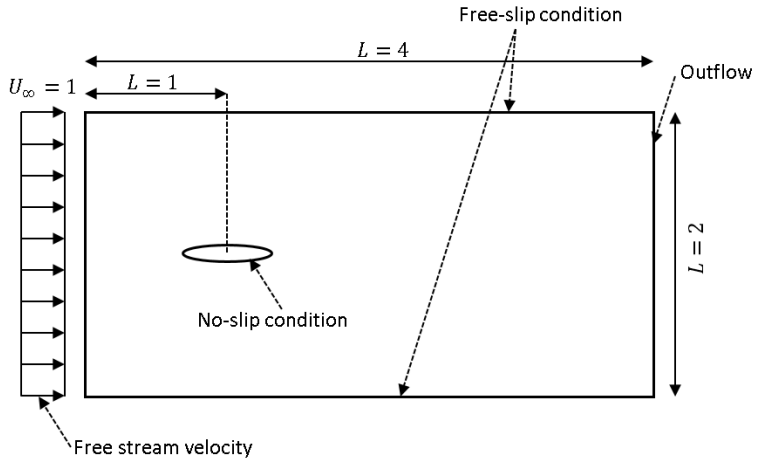

b) Computational domain

Figure 15. Simplified wing model.

The airfoil is defined using the Joukowsky transformation shown in Equation (14). This trans-

formation maps a circle passing through $z_1 = 1$ and containing the point $z_2 = -1$ to a curve shaped like the cross section of an airplane wing. The Joukowsky transformation is done in a complex plane.

$$J(z) = z + \frac{1}{z} \quad , \quad z = x + iy \tag{14}$$

By changing the center location of the original circle, it is possible to change the airfoil camber. The effect of change in the center location of the original circle on the camber and thickness of the airfoil is shown in Figure 16. It should be noted that after generation, the airfoils are normalized such that the chord length is always equal to one.

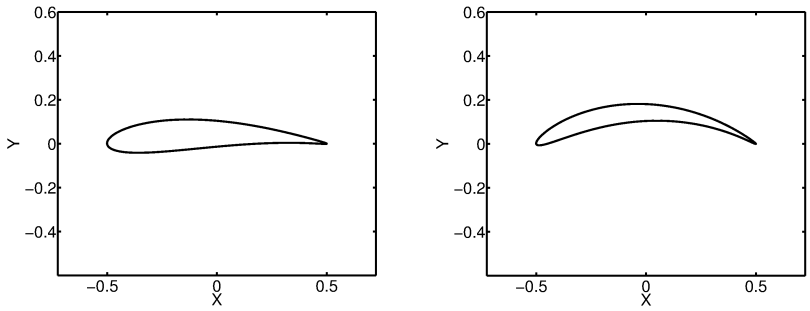

a) Original circle at $(-0.1, 0.1)$ **b) Original circle at** $(-0.05, 0.3)$

Figure 16. Airfoil definition by Joukowsky transformation (not normalized).

The pressure and u-velocity contour plots for the flow over the airfoils are shown in Figure 17. We refer to the airfoil shown in Figure 16a as J_1 and Figure 16b as J_2.

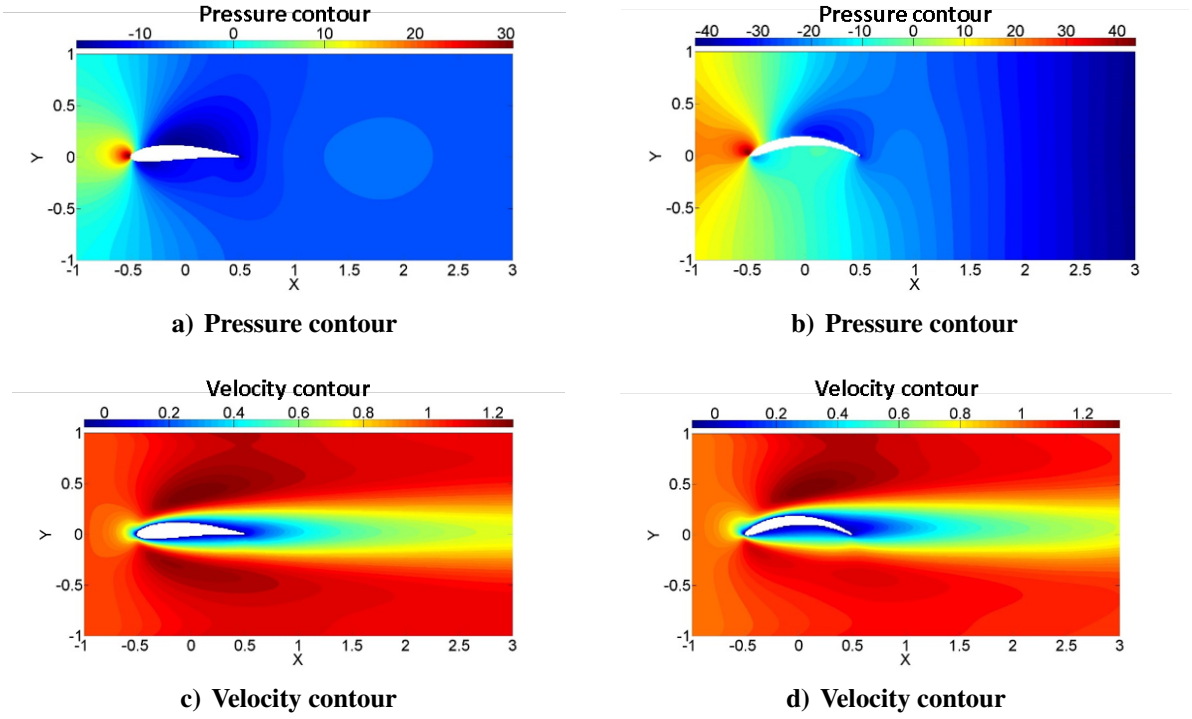

a) Pressure contour **b) Pressure contour**

c) Velocity contour **d) Velocity contour**

Figure 17. Airfoil definition by Joukowsky transformation (not normalized).

As shown in Figure 18 the feedback forcing function is able to bring the velocity to zero on the surface of the airfoil.

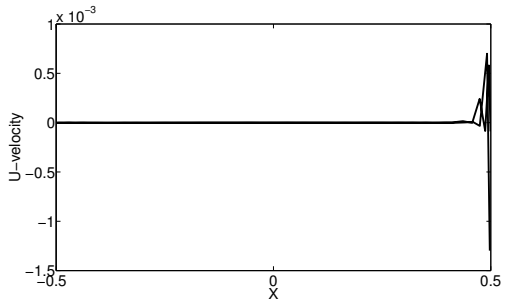

a) U-velocity on J_1 airfoil

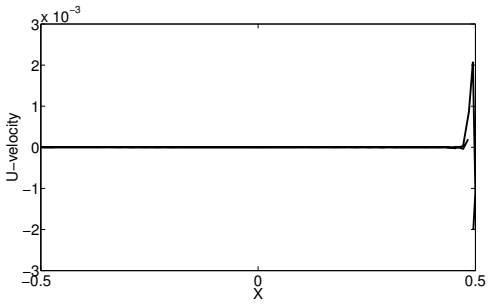

b) U-velocity on J_2 airfoil

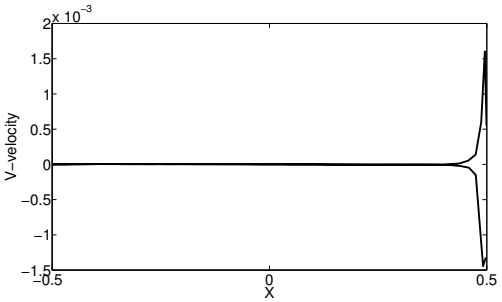

c) V-velocity on J_1 airfoil

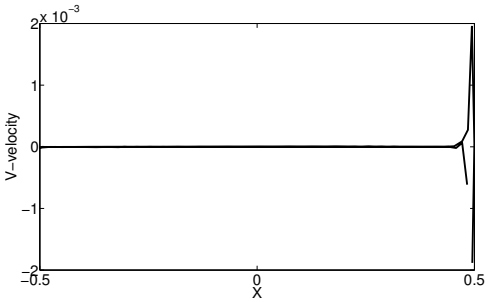

d) V-velocity on J_2 airfoil

Figure 18. Flow velocity on the surface of airfoils defined in Figure 16.

The governing equations, along with the boundary conditions, are differentiated to derive the CSEs as described in the previous section. The resulting system of equations is solved to get the sensitivity response of the system. As shown in Figure 16, the y coordinate of the center of the original circle defines the camber. The tip displacement is proportional to the load on the structure, which itself depends on the integral of the pressure over the surface of the airfoil. Therefore, to calculate the tip displacement sensitivity, it is required to calculate the pressure sensitivity and integrate it over the airfoil boundary.

The pressure field sensitivity on the top and bottom surfaces of the airfoil to camber line variation is shown in Figure 19. The integral of these functions are used to calculate the sensitivity of tip displacement to the change in airfoil camber. We used complex step method to verify the sensitivity results. As shown in Table 1, the results of the continuum sensitivity analysis agrees well with the complex step results.

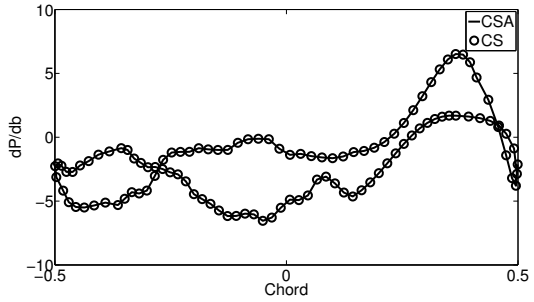

a) J_1 **airfoil**

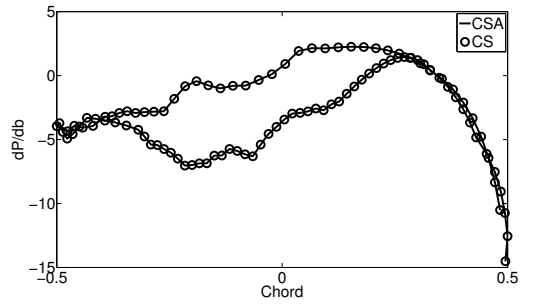

b) J_2 **airfoil**

Figure 19. Pressure sensitivity on the surface of the airfoils.

	CSA	Complex step	airfoil
$d\delta/dy_c$	0.441	0.441	J_1
$d\delta/dy_c$	0.68	0.68	J_2

Table 1. Tip displacement sensitivity to camber

IV. Conclusions

In this research, a continuum sensitivity analysis formulation is developed for the shape sensitivity analysis for the fluid-solid interaction problems. The flow is modelled as an incompressible, laminar, and viscous fluid where the Navier-Stokes equations are used to calculate the fluid response. The solid boundaries are modelled using the continuum formulation of immersed boundary method with an addition of feedback forcing function to the Navier-Stokes equations to represent the effect of solid boundaries. Using this approach, we were able to decouple the fluid mesh from the shape of the solid boundary. This results in improving the robustness of the method since no mesh deformation is needed to handle the solid region movement. Moreover, the sensitivity analysis is simplified since the local and total sensitivities are equal for this formulation. A nonlinear

mapping function is used to couple the fluid and solid domain (Eulerian and Lagrangian) grids and to map the data between these domains. As a requirement for continuum sensitivity analysis, the mapping function used need to be $\mathcal{C}^1$ continuous. This is satisfied by proposing a novel regularized delta function that has continuous derivatives. The applicability of the proposed function is showed in this research.

This methodology is applied to two different demonstration problems. For the first problem, the sensitivity of flow to change in the radius of an immersed cylinder is calculated. The results show a good comparison with the complex step results. It was shown that the method can handle flow with different Reynolds numbers. For the second demonstration problem, the one-way coupling of structural response and the fluid domain is investigated. The sensitivity of the displacement of simplified wing model to the shape of the lifting surface calculated. For this problem, the method was able to calculate accurate sensitivities.

Acknowledgements

The authors would like to acknowledge the support provided by the Air Force Research Laboratory through contract FA8650-09-23938, the Collaborative Center for Multidisciplinary Sciences.

References

[1] Martins, J. R. and Hwang, J. T., "Review and unification of methods for computing derivatives of multidisciplinary computational models," *AIAA Journal*, Vol. 51, No. 11, 2013, pp. 2582–2599.

[2] Cross, D. M. and Canfield, R. A., "Local continuum shape sensitivity with spatial gradient reconstruction," *Structural and Multidisciplinary Optimization*, Vol. 50, No. 6, 2014, pp. 975–1000.

[3] Peter, J. E. V. and Dwight, R. P., "Numerical sensitivity analysis for aerodynamic optimization: A survey of approaches," *Computers & Fluids*, Vol. 39, No. 3, 2010, pp. 373–391.

[4] Arora, J. and Haug, E., "Methods of Design Sensitivity Analysis in Structural Optimization," *AIAA Journal*, Vol. 17, No. 9, 1979, pp. 970–974.

[5] Dems, K. and Mroz, Z., "Variational approach to first- and second-order sensitivity analysis of elastic structures," *International Journal for Numerical Methods in Engineering*, Vol. 21, No. 4, 1985, pp. 637–661.

[6] Stanley, L. G. D. and Stewart, D. L., *Design Sensitivity Analysis: Computational Issues of Sensitivity Equation Methods*, Frontiers in applied mathematics, Society for Industrial and Applied Mathematics (SIAM, 3600 Market Street, Floor 6, Philadelphia, PA 19104), 2002.

[7] Etienne, S. and Pelletier, D., "A general approach to sensitivity analysis of fluid–structure interactions," *Journal of fluids and structures*, Vol. 21, No. 2, 2005, pp. 169–186.

[8] Liu, S. and Canfield, R. A., "Equivalence of continuum and discrete analytic sensitivity methods for nonlinear differential equations," *Structural and Multidisciplinary Optimization*, Vol. 48, No. 6, 2013, pp. 1173–1188.

[9] Sahin, M. and Mohseni, K., "An arbitrary Lagrangian–Eulerian formulation for the numerical simulation of flow patterns generated by the hydromedusa Aequorea victoria," *Journal of Computational Physics*, Vol. 228, No. 12, 2009, pp. 4588–4605.

[10] Liu, S. and Canfield, R. A., "Boundary velocity method for continuum shape sensitivity of nonlinear fluid–structure interaction problems," *Journal of Fluids and Structures*, Vol. 40, No. 0, 2013, pp. 284 – 301.

[11] Mittal, R. and Iaccarino, G., "Immersed boundary methods," *Annu. Rev. Fluid Mech.*, Vol. 37, 2005, pp. 239–261.

[12] Choi, J.-I., Oberoi, R. C., Edwards, J. R., and Rosati, J. A., "An immersed boundary method for complex incompressible flows," *Journal of Computational Physics*, Vol. 224, No. 2, 2007, pp. 757–784.

[13] Fadlun, E., Verzicco, R., Orlandi, P., and Mohd-Yusof, J., "Combined immersed-boundary finite-difference methods for three-dimensional complex flow simulations," *Journal of Computational Physics*, Vol. 161, No. 1, 2000, pp. 35–60.

[14] Mittal, R., Dong, H., Bozkurttas, M., Najjar, F., Vargas, A., and von Loebbecke, A., "A versatile sharp interface immersed boundary method for incompressible flows with complex boundaries," *Journal of computational physics*, Vol. 227, No. 10, 2008, pp. 4825–4852.

[15] Challis, V. J. and Guest, J. K., "Level set topology optimization of fluids in Stokes flow," *International journal for numerical methods in engineering*, Vol. 79, No. 10, 2009, pp. 1284–1308.

[16] Kreissl, S. and Maute, K., "Levelset based fluid topology optimization using the extended finite element method," *Structural and Multidisciplinary Optimization*, Vol. 46, No. 3, 2012, pp. 311–326.

[17] Goldstein, D., Handler, R., and Sirovich, L., "Modeling a no-slip flow boundary with an external force field," *Journal of Computational Physics*, Vol. 105, No. 2, 1993, pp. 354–366.

[18] Shin, S. J., Huang, W.-X., and Sung, H. J., "Assessment of regularized delta functions and feedback forcing schemes for an immersed boundary method," *International Journal for Numerical Methods in Fluids*, Vol. 58, No. 3, 2008, pp. 263–286.

[19] Gobal, K., Grandhi, R. V., and Kolonay, R. M., "Continuum Sensitivity Analysis for Structural Shape Design Variables Using Finite-Volume Method," *AIAA Journal*, Vol. 53, No. 2, 2014, pp. 347–355.

[20] Brown, D. L., Cortez, R., and Minion, M. L., "Accurate projection methods for the incompressible Navier–Stokes equations," *Journal of computational physics*, Vol. 168, No. 2, 2001, pp. 464–499.

[21] Martins, J. R., Sturdza, P., and Alonso, J. J., "The complex-step derivative approximation," *ACM Transactions on Mathematical Software (TOMS)*, Vol. 29, No. 3, 2003, pp. 245–262.